THE ASTROPHYSICAL JOURNAL, 475:11–19, 1997 January 20
© 1997. The American Astronomical Society. All rights reserved. Printed in U.S.A.

AN X-RAY AND OPTICAL STUDY OF MATTER DISTRIBUTION IN CLUSTERS OF GALAXIES

GIUSEPPE CIRIMELE, ROBERTO NESCI, AND DARIO TRÈVESE
Istituto Astronomico, Università di Roma "La Sapienza," via G. M. Lancisi 29, I-00161 Roma, Italy;
cirimele@astrm2.rm.astro.it, nesci@astrm2.rm.astro.it, trevese@astrm2.rm.astro.it
Received 1996 June 17; accepted 1996 August 13

ABSTRACT

A sample of 12 Abell clusters of galaxies has been studied in the optical and X-ray bands. The optical data are derived from automatic photometry based on microdensitometric scans of Palomar Schmidt F-band plates. *ROSAT* PSPC data were obtained from the public archive. Galaxy density and X-ray luminosity profiles have been constructed and deprojected by parametric and nonparametric techniques to obtain volume density profiles. We find a relation between the gas density $\rho_{\rm gas}$ and the galaxy density $\rho_{\rm gal}$ consistent with the prediction of the hydrostatic isothermal model. We confirm that more than 70% of the cluster mass is dark within 1.5 Mpc h_{50}^{-1} from the cluster center. Outside 250 kpc we find a nearly constant M/L_V ratio, which on average is 137 $M_\odot/L_\odot$, implying that the galaxy mass traces the total matter distribution. The dark mass-to-light ratio has a similar behavior. We also find a baryonic fraction $f_b \approx 0.2$, which, assumed as representative of the cosmic value and compared with nucleosynthesis calculations, constrains the cosmological parameter Ω_0 to be smaller than 0.25.

Subject headings: dark matter — galaxies: clusters: general — galaxies: photometry — methods: statistical — X-rays: galaxies

1. INTRODUCTION

X-ray studies of galaxy clusters provide various key pieces of information to understand the nature, the physical state, and possibly the origin and evolution of these objects. The distribution of the total mass of clusters and the ratio between gas, galaxy, and dark matter are particularly relevant for cosmological studies. Mass estimates based on the distribution of galactic redshifts provide only model-dependent estimates of the cluster binding masses. The uncertainty can even reach 1 order of magnitude, being dependent on the assumptions that (1) the system is in virial equilibrium, (2) the velocity distribution is isotropic, and (3) the galactic light traces the mass distribution.

More information can be obtained from X-ray data. According to the current interpretation of the X-ray observations, thermal bremsstrahlung radiation is produced by the hot gas, which is in hydrostatic equilibrium in the gravitational field of the total matter in the cluster: gas, stellar, and baryonic and nonbaryonic dark matter. In this framework it is possible to derive the spatial distribution of both the total mass and the gas mass, from the X-ray surface brightness and the temperature profile, deduced from the radiation spectrum (Sarazin 1988). From these distributions it is possible to infer the global baryonic mass fraction f_b of the universe, which, together with the estimate of the baryon density parameter Ω_b derived from the studies of the primordial nucleosynthesis, allows us to constrain the density parameter $\Omega_0 = \Omega_b/f_b$ (White 1992; White et al. 1993).

X-ray data have been used by several authors to obtain mass estimates of clusters of galaxies (e.g., Cowie, Henriksen, & Mushotzky 1987; Hughes, Gorenstein, & Fabricant 1988; Gerbal et al. 1992). Combined optical and X-ray data have been used to derive simultaneously the masses of the gas, galaxies, and dark matter (e.g., Hughes 1989; Eyles et al. 1991; Briel, Henry, & Böhringer 1992; Durret et al. 1994; David, Jones, & Forman 1995). From these works the gas distribution appears more spatially extended than the distribution of galaxies and dark matter. There are evidences of a greater central concentration of the dark matter with respect to the luminous mass (Durret et al. 1994), which are consistent with the estimates based on studies of gravitational lensing (e.g., Tyson, Valdes, & Wenk 1990; Smail et al. 1995).

According to David et al. (1995) the mass-to-light ratio is $M/L_V \sim 100$–$150\ M_\odot/L_\odot$ (see also Cowie et al. 1987), i.e., smaller than the previous estimate based on galaxy velocities. Furthermore, a baryon fraction $f_b \geq 0.11\ h_{50}^{-3/2}$ implies $\Omega_0 \simeq 0.1$–0.2 assuming $\Omega_b \simeq 0.05\ h_{50}^{-2}$ from nucleosynthesis calculations (Walker et al. 1991). The errors on the mass estimate are mainly caused by the uncertainties in the temperature determination.

The present limitation of X-ray data for the study of rich and hot galaxy clusters is the lack of spatially resolved spectra. In fact, both the *Einstein* imaging proportional counter (IPC) and the *ROSAT* position-sensitive proportional counter (PSPC) instruments, which have the highest angular resolution, have low spectral resolution and detect photons with energies below 4.0 and 2.4 keV, respectively, so they cannot give reliable measurements of the temperature profile of hot ($T \gtrsim 3$ keV) clusters. On the other hand, instruments with better spectral coverage and resolution, such as *ASCA*, have a much lower spatial resolution ($\approx 2'$), which is only adequate for nearby ($z \lesssim 0.1$) clusters.

The accuracy of the cluster binding mass estimate derived from X-ray observations has been recently investigated by Schindler (1996). For simulated *ROSAT* observations of regular clusters she obtains uncertainties smaller than 10% within 2 Mpc from the center. This result has been confirmed by Evrard, Metzler, & Navarro (1995) on the basis of various galaxy clustering simulations, showing that in most cases clusters are isothermal or exhibit moderate temperature gradients within regions of average densities greater than 500 times the cosmic critical density ρ_c.

In the present study we analyze the matter distribution in

a sample of 12 clusters using both optical data from our previous studies (Trèvese et al. 1992b; Flin et al. 1995) and *ROSAT* PSPC public X-ray data. We assume a constant temperature, we limit the analysis to the inner 1.5 Mpc, and we compare the results with the literature. The paper is organized as follows: in § 2 we present the X-ray and optical data, with the relevant reduction procedures and remarks on individual clusters; in § 3 we discuss the assumption of the hydrostatic equilibrium and we analyze the binding mass and the different components of matter.

We use $H_0 = 50$ km s^{-1} Mpc^{-1} and $q_0 = \frac{1}{2}$ throughout.

2. DATA AND REDUCTIONS

The main aim of the present work is to combine the information obtained from X-ray and optical data to study the spatial distribution of the various kinds of matter. In the past we have carried out an optical study of about 50 Abell clusters of galaxies, analyzing their morphologies and the luminosity functions (Trèvese et al. 1992a, 1992b; Trèvese, Cirimele, & Appodia 1996). *ROSAT* PSPC data are the best suited for this kind of analysis because of their good spatial resolution. We then searched the *ROSAT* public archive for X-ray observations of the clusters of our sample. We excluded off-axis observations because of their lower resolution (Hasinger et al. 1993). The cross-correlation of the optical and X-ray lists produced a sample of 12 clusters described in Table 1.

TABLE 1

CLUSTER SAMPLE

Abell Number	z	M_F^*	N_H (10^{20} cm^{-2})	RS	T (keV)
76	0.0416	−22.73	3.85	L	1.5
119	0.0440	−22.71	3.45	cD	5.9
1377.....	0.0514	−22.73	2.16	B	3.3
1413.....	0.1427	−22.32	1.98	cD	7.3
1689.....	0.1832	−23.39	1.87	C	10.1
1775.....	0.0717	−23.17	1.07	B	4.9
2052.....	0.0348	−22.08	2.91	cD	3.1
2063.....	0.0337	−22.03	2.91	cD	4.1
2199.....	0.0303	−21.90	0.87	cD	4.5
2634.....	0.0312	−21.48	4.94	cD	3.4
2657.....	0.0414	−22.59	6.00	F	3.4
2670.....	0.0745	−22.73	2.69	cD	3.9

NOTE—T is from David et al. 1993; for A1377 the temperature has been estimated in the present work. N_H is from Stark et al. 1992. RS is the Rood & Sastry 1971 morphological type.

2.1. *X-Ray Data*

We used images in the hard band 0.4–2.4 keV with 15″ pixel size extracted from the public archive of the Goddard Space Flight Center. We corrected the images for exposure variations and telescope vignetting using exposure maps generated with the code of Snowden et al. (1992; see also Plucinsky et al. 1993).

In order to reduce systematic errors in the cluster mass distribution, we have removed by visual inspection obvious discrete external sources superimposed on the clusters.

Cluster centers were determined with an iterative procedure computing the first moment of the X-ray images in circular areas of fixed radius of about 1 Mpc, starting from the intensity peak and locating the point where the variations of the center coordinates are smaller than the pixel size.

In order to determine the gas density profile, we assumed spherical symmetry and we computed a radial brightness profile using annular bins of 15″. A constant background value (I_b) was evaluated in the outer regions of each cluster (outside $b = 3$ Mpc; see Table 2) and subtracted from the radial profile.

The radial brightness profiles were deprojected in two different ways: (1) by a nonparametric deprojection using the Abel integral,

$$I(r) = -\frac{1}{2\pi r}\frac{d}{dr}\int_{r^2}^{\infty}\frac{I(b)db^2}{\sqrt{b^2 - r^2}},$$

and (2) by a parametric deprojection obtained through a fit of the data with a King profile,

$$I(b) = I_0[1 + (b/r_c)^2]^{-3\beta+0.5},$$

convolved with a Gaussian filter with $\sigma = 15''$ to take into account the *ROSAT* point-spread function (psf). The deprojected density is then obtained analytically.

The accuracy of method 1 has been tested through simulations of clusters with a King profile convolved with a Gaussian psf with standard deviation $\sigma = 1$ pixel. The procedure applied to the simulated spherically symmetric clusters shows that the error is less than 5% within a radius of 1.5 Mpc, using an integration upper limit of 3 Mpc.

The fit was performed inside a region $r < 1.5$ Mpc around the cluster center. Data bins with low signal-to-noise ratio were collected together at large radii where the psf becomes wider than 30″. We checked that the convolution with the psf affects the estimates of the fit parameters by less than 5%.

The presence of a cooler gas component in the central region turns out to be one of the main causes of uncertainty. The correct determination of the background value is also particularly important, since even small variations may cause a spread in the fitting parameters. Table 2 summarizes the results of the fits and the relevant goodness.

As an example, Figure 1 shows the gas density distributions of the cluster A1413, obtained with the two methods, which in general are in good agreement. Sometimes differences appear in the central part, where the King profile fails to describe the actual gas density distribution, owing to the presence of a cooling flow. In these cases the fit has been repeated excluding the central part, as specified in § 2.3.

The value of the central gas density and the normalization of the nonparametric deprojected profile were obtained assuming a Raymond-Smith (1977) spectrum with a constant cluster temperature taken from David et al. (1993) (see Table 1). In each case the spectrum has been corrected for extinction using column density data from Stark et al. (1992).

We have compared our results with those obtained by Jones & Forman (1984) from *Einstein* data, for the clusters A1377, A1775, A2063, A2199, A2634, A2657, and A2670. Overall, the comparison indicates a good agreement. For n_0 the agreement is better than for r_c and β. Our central densities are also in agreement with those found from Abramopoulos & Ku (1983), in the case of A119 and A2052. We have also three clusters (A1689, A2657, and A2670) in common with Durret et al. (1994), who used *Einstein* data. In this case the agreement is poor. In particular, they obtain smaller core radii. However, they also find systematically

TABLE 2

X-Ray Fitting Parameters

Abell Number	Sequence Identification	Exposure Time (s)	$I_b \times 10^4$ (counts s^{-1} $arcmin^{-2}$)	$n_0 \times 10^3$ (cm^{-3})	r_c (kpc)	β	χ^2/ν
76	rp800317	1697	2.5	1.07	356	0.58	25/18
119	rp800251	15203	3.0	1.18	378	0.56	56/50
1377.....	rp800106	4971	6.2	0.75	188	0.46	12/18
1413.....	wg800183	11364	2.7	8.00	156	0.62	12/19
1689.....	rp800248	13957	4.0	14.04	205	0.72	22/19
1775.....	wg701068	12921	2.9	2.73	174	0.58	61/42
2052.....	rp800275	6215	7.3	4.43	142	0.67	45/45
2063.....	wg800184	14888	4.4	5.9	74	0.50	37/37
2199.....	wp150083	21208	3.5	6.5	117	0.62	60/51
2634.....	rp800014	9866	4.0	0.89	320	0.58	99/42
2657.....	rp800320	18911	1.6	4.4	124	0.52	104/63
2670.....	rp800420	54699	3.8	3.83	174	0.70	37/31

smaller values of the β parameter. As a result, their and our HWHMs are consistent within 30%. They fitted synthetic images to *Einstein* data also taking into account the cluster elongation. This can explain part of the discrepancy, while part can be ascribed to the lower resolution of the *Einstein* data.

From the radial profile of the deprojected gas density we have computed the total gas mass as a function of r, integrating the profile and assuming a constant gas temperature. The results are presented and discussed in § 3.

2.2. *Optical Data*

Our optical data are derived from photographic plates taken by P. Hickson with the 48 inch (1.2 m) Palomar Schmidt telescope to analyze a sample of 64 Abell clusters. The resulting photometry corresponds to the red F band of Oemler (1974). Plates were scanned with a PDS 1010G in Rome, with pixel sizes ranging from 10 to 25 μm according to the cluster distance. Automatic identification of objects and their classification as pointlike or diffuse are described in Trèvese et al. (1992b). Total magnitudes are computed from the flux integrated in a circular aperture whose radius is $R_1 = 1.5r_1$, where r_1 is the first moment of the intensity distribution (see Trèvese et al. 1992b). The magnitude defined in this way corresponds on average to an isophotal magnitude at 24 mag $arcsec^{-2}$. The zero of the magnitude scale has been established using published photometric data.

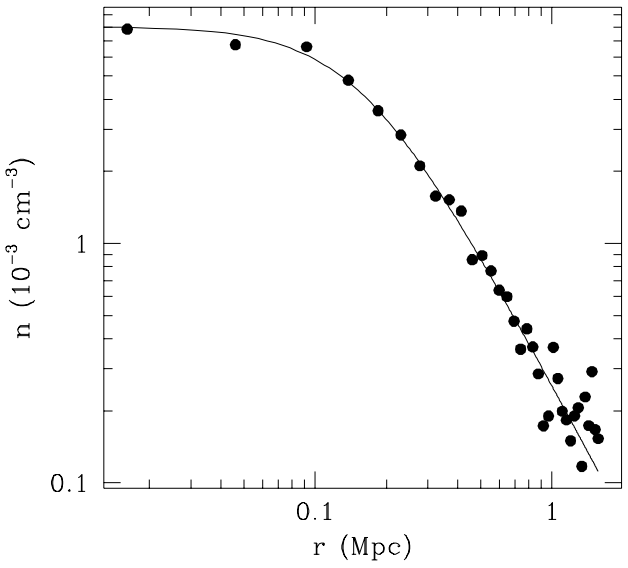

Fig. 1.—Gas density profile for Abell 1413. The points represent the nonparametric deprojection, and the line represents the deprojection obtained by a fit of the surface X-ray brightness.

In almost all cases the optical centers computed from the spatial distribution of galaxies are very close to the X-ray centers, which are adopted as cluster centers.

The galaxies' luminosity distribution has been parameterized by a Schechter function, and the fit has been performed using a maximum likelihood algorithm. This allows us to use unbinned data, and it avoids the introduction of a nonphysical scale related to the choice of the bin width. Table 1 reports the value of M^* for eight clusters taken from Trèvese et al. (1996) and obtained with a fixed parameter $\alpha = -1.25$. Four other clusters, A119, A2063, A2199, and A2634, have been analyzed in the present work, and the relevant M^* values have been computed with the same algorithm. Details on individual clusters are reported in § 2.3. The spatial distribution of galaxies has been fitted with a King profile, $\sigma_{\rm gal} = \sigma_0[1 + (r/r_c)^2]^{-\delta} + \sigma_b$, using r_c, β, and σ_b as free parameters, while σ_0 is determined by normalization to the observed galaxy number.

A different representation of the projected galaxy distribution can be obtained using a de Vaucouleurs profile, $\sigma_{\rm gal} = \sigma_0 \exp\,[-(r/r_v)^\gamma] + \sigma_b$, where again the constant background galaxy counts σ_b, r_v, and γ are free parameters. The fit has been performed using the brightest galaxies in a range of about 2 mag (see Table 3) inside a region of 2 Mpc radius. The value of σ_b obtained from the fit was compared with the field galaxy counts in the same magnitude range. In almost all cases, σ_b and background count values are very similar. For two clusters, A1413 and A1775, that show evident substructure the background has been estimated from the outer region and has been fixed in the maximization procedure. The goodness of fit has been tested using the Kolmogorov-Smirnov (KS) test applied to the cumulative distributions. The results of the fitting analysis are reported in Table 3.

At least in the present cluster sample, the de Vaucouleurs profile provides a better fit to the galaxy number density distribution with respect to the King profile, particularly

TABLE 3

OPTICAL RESULTS

	de Vaucouleurs					King					
Abell Number	σ_0 (kpc^{-2})	r_v (kpc)	γ	σ_b (kpc^{-2})	P_{KS} ($>D$)	σ_0 (kpc^{-2})	r_c (kpc)	δ	σ_b (kpc^{-2})	P_{KS} ($>D$)	M_{lim}
76	0.39×10^{-4}	485	0.678	0.18×10^{-6}	0.83	0.34×10^{-4}	469	0.89	0.33×10^{-6}	0.81	−20.5
119	0.21×10^{-3}	448	0.271	0.61×10^{-6}	0.87	0.41×10^{-4}	375	0.57	0.76×10^{-6}	0.85	−21.0
1377.....	0.23×10^{-4}	97	0.251	0.75×10^{-7}	0.81	0.16×10^{-4}	181	0.91	0.85×10^{-6}	0.88	−21.2
1413.....	0.16×10^{-4}	34	2.075	0.71×10^{-5}	0.26	0.62×10^{-4}	232	1.02	0.71×10^{-5}	0.03	−21.5
1689.....	0.14×10^{-3}	211	0.430	0.61×10^{-6}	0.84	0.37×10^{-4}	296	0.84	0.69×10^{-6}	0.85	−22.5
1775.....	0.21×10^{-3}	685	0.227	0.70×10^{-6}	0.38	0.47×10^{-4}	84	0.34	0.70×10^{-6}	0.36	−21.3
2052.....	0.17×10^{-3}	82	0.553	0.19×10^{-5}	0.88	0.92×10^{-4}	139	0.70	0.23×10^{-5}	0.66	−21.2
2063.....	0.15×10^{-3}	198	0.767	0.54×10^{-6}	0.91	0.85×10^{-4}	253	0.94	0.54×10^{-6}	0.96	−21.2
2199.....	0.44×10^{-3}	120	0.264	0.11×10^{-5}	0.98	0.78×10^{-4}	206	0.61	0.65×10^{-6}	0.69	−21.0
2634.....	0.46×10^{-3}	65	0.252	0.56×10^{-7}	0.82	0.47×10^{-3}	340	0.47	0.45×10^{-7}	0.60	−20.5
2657.....	0.65×10^{-3}	470	0.344	0.15×10^{-5}	0.92	0.24×10^{-3}	90	0.98	0.59×10^{-5}	0.59	−20.3
2670.....	0.25×10^{-3}	130	0.393	0.49×10^{-6}	0.62	0.51×10^{-4}	340	0.85	0.49×10^{-6}	0.67	−21.4

within 1 Mpc from the center. The higher central density of the de Vaucouleurs with respect to the King profile could indicate an excess of radial orbits in the cluster center, as suggested by Tonry (1985). The effect would even be enhanced by the mass segregation, which is not taken into account in the present fits of the number density profiles. From the projected galaxy distribution we derived the corresponding three-dimensional profile and, by integration, the total galactic mass of the cluster as a function of r.

In order to compare our results with the literature, we have adopted for the stellar mass-to-light ratio $M/L_V = 8\ M_\odot/L_\odot$ (David et al. 1990) after the transformation $V = F + 0.76$, appropriate from bright elliptical galaxies (Schneider, Gunn, & Hoessel 1983). To compute the total luminosity in a fixed volume, we extrapolated the luminosity function (LF) to faint magnitude using the fixed-α Schechter LF. This gives

$$L_{tot}(r) = 10^{-0.4(M_F^* + 28.43)} \frac{4\pi\Gamma(2+\alpha)}{\Gamma(1+\alpha, L_{lim}/L^*)} \int_0^r \rho_{gal}(r') r'^2\, dr' , \quad (1)$$

where L_{tot} is expressed in units of $10^{13}\ L_\odot$, r in kiloparsecs, and L_{lim} is the limiting luminosity reported in Table 3 as M_{lim}.

It is important to check whether the results are affected by the particular parameterization of the density profile. However, unlike the case of X-ray data, the galaxy density can hardly be deprojected by a nonparametric method. In fact, galaxy number counts are affected by Poissonian fluctuations that cannot be reduced by a longer exposure time as can the fluctuations of X-ray photon counts.

Thus we have directly compared the projected galaxy mass distribution with the projected gas and total mass distributions. In this case the galaxy mass profile is simply obtained from counts in circular areas after subtraction of the relevant background counts. This galaxy mass distribution will be compared with the projected gas mass in § 3.3.

2.3. *Remarks on Individual Clusters*

Abell 76.—This is an F cluster observed with *ROSAT* for only 1697 s, but the X-ray brightness profile allows a reliable estimate of the gas density. The optical and X-ray images appear more regular than expected for this cluster type, and the position angle of the cluster is 90° in both X-ray and optical images. The temperature value $T = 1.6$ keV is the most uncertain among Abell clusters in the David et al. (1993) list.

Abell 119.—Two discrete sources at 12′ and 22′ distance from the center have been removed from the image. The X-ray image exhibits an extension in the northern part. The optical image of this cluster is very regular in the central part and shows an extension similar to the X-ray image. The best estimate of the Schechter parameter M^*, found using the same algorithm of Trèvese et al. (1996), is $M^* = -22.70 \pm 0.15$ at the 1 σ level.

Abell 1377.—The X-ray image of this cluster is very faint and shows several discrete emission sources in the field. We have removed the source at 7.′8 and at 11.′5 from the cluster center. The comparison between X-ray and optical images reveals an identical morphology with a positional angle of 80°. A temperature value of 3.3 keV has been estimated from the PSPC spectrum, since it was not found in the literature.

Abell 1413.—Two small discrete sources were removed from the X-ray image at 4.′8 and 5.′6 from the center. This cluster appears very regular in the X-ray image, but the optical counterpart, although it is extremely similar, shows a subcluster in the west side at 5′ (0.9 Mpc) from the center. This is likely due to a projection effect of a background group of galaxies. The fit of the galaxy density distribution is made difficult by the presence of this substructure, and it has been necessary to fix the background value in the fitting procedure.

Abell 1689.—This is the most distant cluster in our sample. The X-ray and optical images are elongated in slightly different directions, possibly as the result of projection effects. The optical sample becomes incomplete at about $m_3 + 2$. Gravitational distortion of background galaxies has been reported in this cluster by Tyson et al. (1990). The central part, within $r < 50$ kpc, has been excluded from the fit of the X-ray brightness.

Abell 1775.—The X-ray image of this cluster differs from the optical one, since a subcluster in the galaxy distribution is present at distance $r = 10'$ from the center. Eight external sources roughly aligned in the southeast direction have been eliminated from the X-ray image. The background galaxy density has been fixed in the fit, owing to the presence of subclustering, as in the case of A1413.

Abell 2052.—We removed a source in the northeast corner at a distance $r = 13.'8$ from the center. The optical

and X-ray images are very similar. The fit of the X-ray brightness has been performed excluding the central $r < 100$ kpc part, due to the presence of a cooling flow.

Abell 2063.—For this cluster our optical data are limited to 1 Mpc from the center. For this reason the galaxies distribution has been fitted fixing the background density to a value determined from a nearby field. Three sources were removed at radius 4′.1, 6′.5, and 8′.8 from the center. Optical and X-ray images are very similar, showing the same substructure at the northeast corner, but the optical image does not reveal the inner substructure in the southwest part appearing in the X-ray image. The fit with fixed $\alpha = -1.25$ of the LF in the magnitude range $-24.0 < M < -19.0$ gives $M^* = -22.02 \pm 0.12$.

Abell 2199.—The Schechter parameter $M^* = -21.9 \pm 0.17$ has been obtained using a magnitude range $-24.0 < M < -19.0$ fixing α to -1.25. Both optical and X-ray images do not show substructures indicating that this is a relaxed cluster. From the fit of the X-ray brightness profile we have excluded the inner 100 kpc containing a cooling flow.

Abell 2634.—We have removed two sources within 15′ from the center. From the fit of the X-ray brightness we excluded the inner 100 kpc containing a cooling flow. $M^* = -21.48 \pm 0.19$ has been obtained fitting the LF in the magnitude range $-23.85 < M \leq -20.5$.

Abell 2657.—We have removed four bright sources at distances of 7′.2, 7′.8, 8′.2, and 15′ from the cluster center. The optical image of this cluster appears more regular than the X-ray image.

Abell 2670.—The X-ray image of this cluster shows evidence of a double peak in the emission revealing a substructure inside the cluster. We have excluded from the image two sources at distances 12′.5 and 17′.5 from the center.

3. THE MATTER DISTRIBUTIONS

The information about the spatial distribution of the various kind of matter in galaxy clusters is usually derived under the assumption of hydrostatic equilibrium of the various components.

3.1. *The Hydrostatic Equilibrium*

The condition that both gas and galaxies are in hydrostatic equilibrium in the same gravitational field produced by the total binding mass can be written (Bahcall & Lubin 1994):

$$\frac{\mu m_p \sigma_r^2}{kT} = \frac{d\ln \rho_{\rm gas}(r)/d\ln r + d\ln T/d\ln r}{d\ln \rho_{\rm gal}(r)/d\ln r + d\ln \sigma_r^2/d\ln r + 2A}, \quad (2)$$

where σ_r is the radial galaxy velocity dispersion and $A = 1 - (\sigma_t/\sigma_r)^2$ measures the anisotropy of the velocity distribution.

If σ_r and T are constant and $A = 0$, this equation implies $\rho_{\rm gas} \propto \rho_{\rm gal}^{\beta}$, where $\beta = \mu m_p \sigma_r^2/kT$ is a constant representing the ratio between the energy per unit mass in galaxies and gas, respectively (Cavaliere & Fusco-Femiano 1976). The β parameter could be directly identified with $\beta_{\rm fit}$ derived from the fit of $\rho_{\rm gas}$ with a King profile, as far as $\rho_{\rm gal}(x) \propto (1 + x^2)^{-3/2}$, or it can be identified with the "corrected" parameter β_c defined by Bahcall & Lubin (1994).

Deriving $\rho_{\rm gas}(r)$ and $\rho_{\rm gal}(r)$, from the X-ray and optical data respectively, allows us to check the consistency of the hydrostatic isothermal model. Once this condition is verified, it is possible to derive from $\rho_{\rm gas}(r)$, which can be determined more accurately, the distribution of the binding mass. Finally, a comparison with the galaxy mass distribution allows us to study the different spatial concentration of the various components (gas, galaxies, dark matter).

In Figure 2, $\log \rho_{\rm gas}$ is plotted against $\log \rho_{\rm gal}$ for our 12 clusters, using for $\rho_{\rm gas}$ the values deduced from the nonparametric deprojection and for $\rho_{\rm gal}$ the values obtained from a de Vaucouleurs fitting profile (see § 2). It is evident from the figure that there is a wide density range where $\log \rho_{\rm gas}(r)$ increases linearly with $\log \rho_{\rm gal}(r)$. Deviations from a straight line occur both at low and at high density values, but are to some extent expected. Indeed, in the cluster outskirts (low density) the signal-to-noise ratio becomes low and the uncertainties on the background estimate become critical. Close to the cluster center, in the inner ≈ 100 kpc (high density), both $\rho_{\rm gas}$ and $\rho_{\rm gal}$ are ill defined because (1) the presence of cooling flows would require locally a dynamical, nonisothermal model and (2) the mass segregation effect would require a position-dependent mass-to-light ratio for galaxies. Thus, $\log \rho_{\rm gas}$ and $\log \rho_{\rm gal}$ are linearly related wherever they are well defined, the linearity being more strict in the case of more regular clusters. This supports the validity of the hydrostatic isothermal model and allows us to define a new X-ray–optical parameter $\beta_{\rm xo}$ such that $\ln \rho_{\rm gas} = \beta_{\rm xo} \ln \rho_{\rm gal} + \text{const}$, which can be directly compared with $\beta_{\rm spec}$ and $\beta_{\rm fit}$.

Table 4 reports the values of $\beta_{\rm xo}$ computed in the linear region, together with the relevant values of $\beta_{\rm fit}$ and $\beta_{\rm spec}$, which are shown in Figure 3. The linear correlation coefficient between $\beta_{\rm xo}$ and $\beta_{\rm fit}$ is $r = 0.77$, with an associated probability of the null hypothesis $P = 4 \times 10^{-3}$.

Previous evidence in favor of the validity of this model was based on the approximate consistency of the average value of the β parameter, derived from a King profile fitting of the X-ray brightness profiles of a sample of clusters, with $\beta_{\rm spec} \equiv \mu m_p \sigma_r^2/kT$, obtained from X-ray and optical spectral data (see Sarazin 1988). Further evidence has been provided by more recent spatially resolved temperature determinations based on *ROSAT* data, which indicate that the temperature is almost constant within the central ≈ 2 Mpc (e.g., Allen et al. 1995). A recent analysis of *ASCA* observations (Markevitch et al. 1996), although it provides

TABLE 4

VALUES OF THE β PARAMETERS

Abell Number	$\beta_{\rm xo}$	$\beta_{\rm fit}$	$\beta_{\rm spec}$
76	0.81 ± 0.11	0.58 ± 0.03	...
119[a]	0.78 ± 0.09	0.56 ± 0.04	$0.74^{+0.25}_{-0.24}$
1377[b]	0.50 ± 0.09	0.46 ± 0.07	0.44 ± 0.40
1413	0.70 ± 0.10	0.62 ± 0.01	...
1689[b]	0.97 ± 0.07	0.72 ± 0.03	2.38 ± 1.20
1775[b]	1.00 ± 0.09	0.58 ± 0.02	3.14 ± 1.56
2052[a]	0.97 ± 0.10	0.67 ± 0.02	$0.90^{+0.32}_{-0.21}$
2063[a]	0.80 ± 0.12	0.50 ± 0.02	$0.65^{+0.19}_{-0.18}$
2199[a]	0.92 ± 0.08	0.62 ± 0.02	$1.00^{+0.35}_{-0.21}$
2634[a]	0.74 ± 0.10	0.58 ± 0.02	$0.89^{+0.30}_{-0.23}$
2657[b]	0.63 ± 0.08	0.52 ± 0.01	0.79 ± 0.27
2670[a]	0.98 ± 0.15	0.70 ± 0.02	$1.50^{+0.84}_{-0.51}$

NOTE—Errors at 90% confidence level.

[a] $\beta_{\rm spec}$ from Girardi et al. 1996.

[b] σ_r from Struble & Rood 1991.

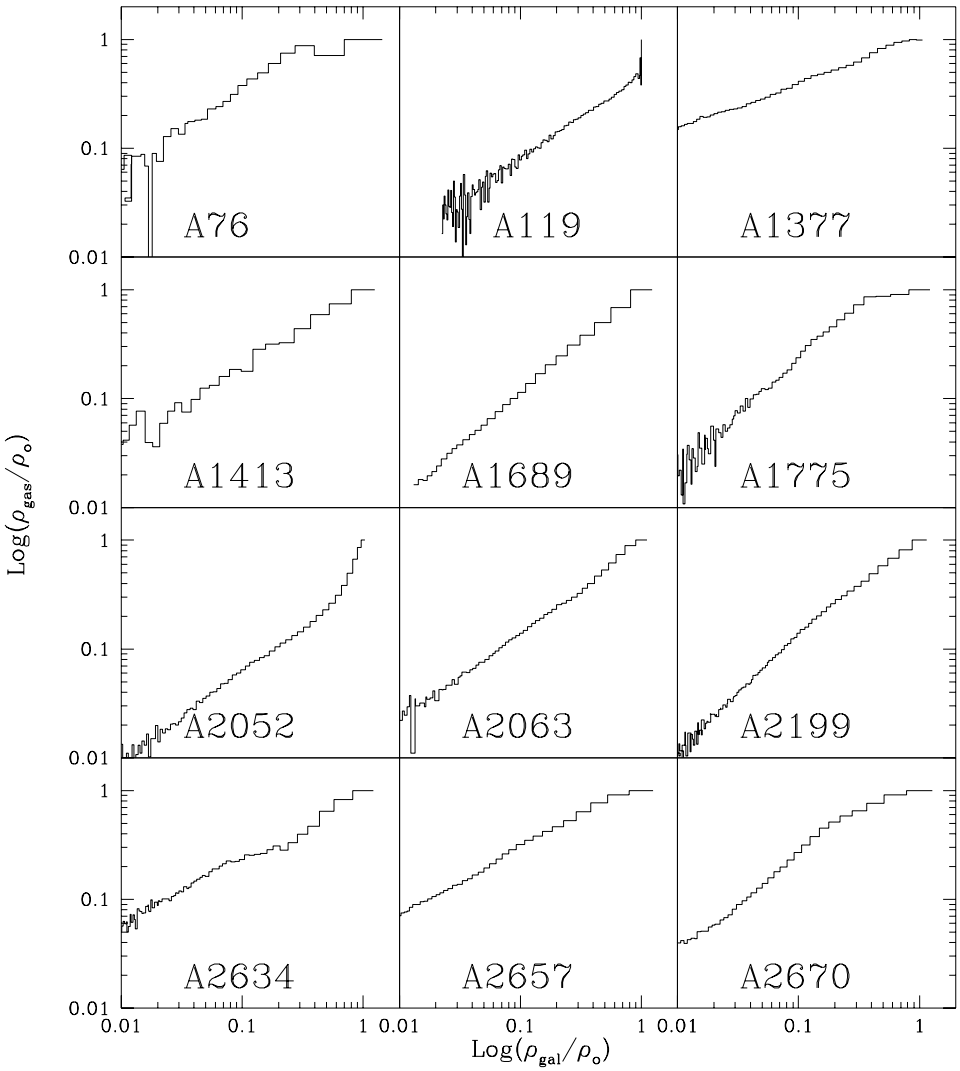

FIG. 2.—Relation between gas and galaxy densities log ρ_{gas} vs. log ρ_{gal} for the entire sample. The slope of the linear portion defines the X-ray–optical β_{xo} parameter.

evidence of a temperature decrease in the outer regions ($r > 2$ Mpc), is consistent with isothermality of the central $r < 1.5$ Mpc.

Our analysis, based on the direct comparison of gas and galaxy density distributions, shown in Figure 2, provides a new evidence in favor of the hydrostatic isothermal model. It is new for two reasons: (1) it is independent of any assumption about the shape of the gas density distribution, and (2) the comparison of gas and galaxy distributions is made within individual clusters and is not based on ensemble averages of β_{spec} and β_{fit}.

3.2. *Determination of the Binding Mass*

We computed the total binding mass profile using the equilibrium equation for the gas (see, e.g., Sarazin 1988):

$$M_{tot}(r) = -\frac{kT}{\mu m_p G}\left[\frac{d\ln\rho_{gas}(r)}{d\ln r} + \frac{d\ln T}{d\ln r}\right] r \,. \qquad (3)$$

In this equation a critical role is played by the derivative of the gas density. Obtaining this quantity from a nonparametric deprojection of the gas density has the advantage of causing no bias in the resulting profile. However, the noise, which is already amplified during the deprojection pro-

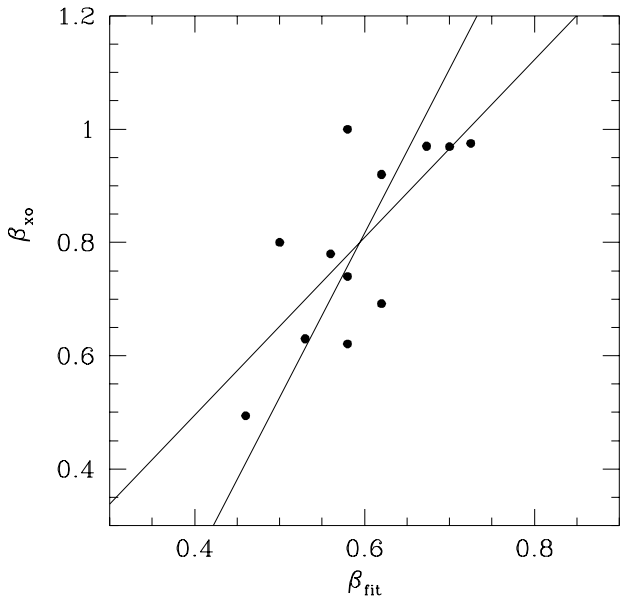

FIG. 3.—X-ray–optical parameter β_{xo} vs. β_{fit}. The regression lines are also shown.

cedure, is further amplified in computing the derivatives in equation (3). This suggests that we use the analytically deprojected density profile. It should also be noted that equation (3), which relates the total binding mass M_{tot} within the radius r with the local gradients, allows us to compute $M_{tot}(r)$ wherever $\rho_{gas}(r)$ is well determined, therefore leaving some uncertainty only at very small radii. To compute $M(r)$, we used the King profile for $\rho_{gas}(r)$ in equation (3), assuming a constant temperature. In this case one gets $M(r) = C\beta_{fit} Tr/[1 + (r_c/r)^2]$, where $C = 1.15$ if r is expressed in kiloparsecs, T in keV, M_{tot} in units of $10^{11} M_\odot$, and the value $\mu = 0.58$ is assumed. In using equation (3), the main source of error on M_{tot} is the uncertainty on T.

The accuracy of the mass estimates based on equation (3) has been recently discussed on the basis of numerical simulations by Schindler (1996), who shows that in regular clusters the uncertainties are smaller than 10% using the β model. A similar result is found by Evrard et al. (1995).

3.3. *Analysis of the Mass Components*

Figure 4 reports the distribution of M_{tot}, M_{gas}, and M_{gal} as functions of radius for the 12 clusters. The values at $r = 1.5$ Mpc are listed in Table 5 together with the relevant total mass-to-light ratio. It can be noted from Figure 4 that $M_{tot}(r)$ and $M_{gal}(r)$ have almost the same slope. The gas mass is more spatially extended, with values that are intermediate between galaxy mass and total binding mass. A

TABLE 5

CLUSTER MASSES

Abell Number	M_{gal} ($10^{13} M_\odot$)	M_{gas}	M_{tot}	M/L_V ($M_\odot/L_\odot$)
76	1.5	5.9	14.4	76
119	3.2	8.4	53.1	134
1377.....	3.0	3.2	25.7	68
1413.....	2.7	12.7	74.0	215
1689.....	4.9	14.4	118.0	192
1775.....	1.7	5.6	46.3	213
2052.....	2.4	4.4	34.0	115
2063.....	2.4	5.1	33.7	113
2199.....	2.2	5.4	46.2	167
2634.....	3.4	4.7	32.4	76
2657.....	2.1	5.5	30.3	117
2670.....	2.4	5.5	46.5	156

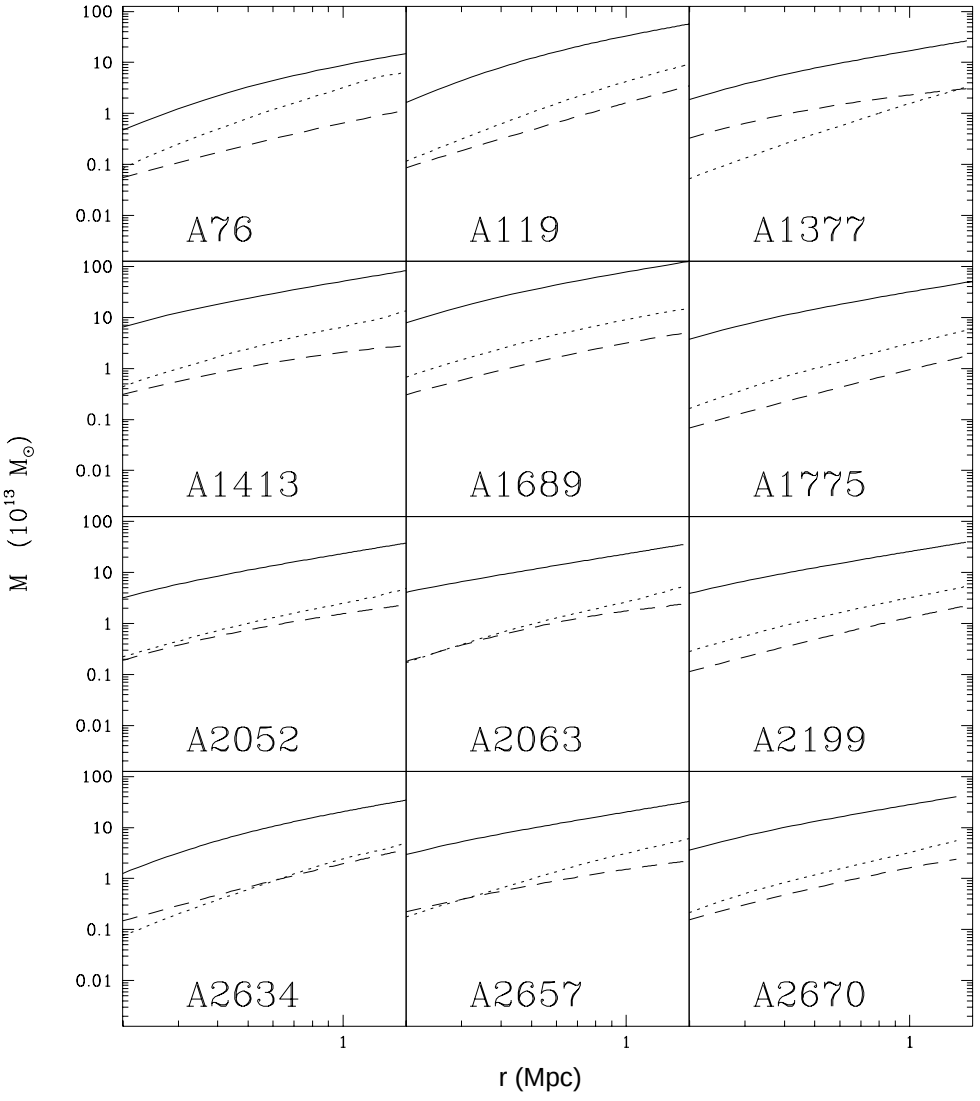

FIG. 4.—Mass as a function of distance for the 12 Abell clusters of the sample. *Solid line:* total binding mass; *dotted line:* gas mass; *dashed line:* galaxy mass.

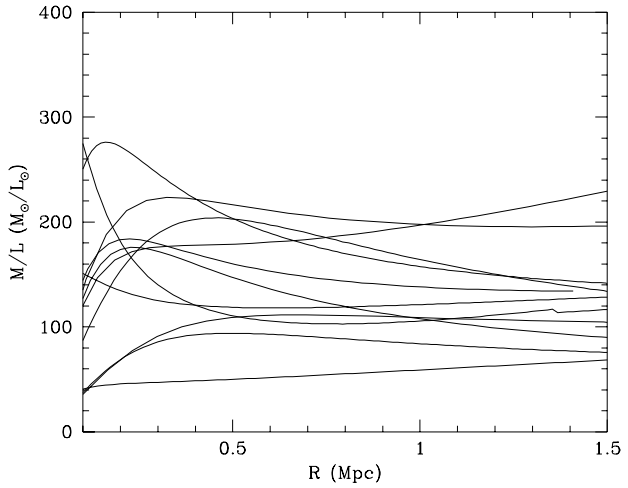

FIG. 5.—Ratio M/L_V in units of $M_\odot/L_\odot$ as a function of radius for the 12 clusters of the sample.

similar behavior was first pointed out by Cowie et al. (1987), subsequently by Hughes (1989) and Eyles et al. (1991) for the Coma and Perseus clusters, and recently by Durret et al. (1994) for A1795, A1991, and A2142 and by David et al. (1995) for a sample of Abell clusters and galaxy groups.

Beyond the qualitative agreement, there are significant variations among individual clusters of different mass, size, and temperature. A better comparison can be obtained by studying the ratios among the various mass components, combined according to the different physical aspects of interest.

For comparison with previous studies, let us consider first the mass-to-light ratio M/L_V as a function of radius. Two features clearly appear from Figure 5: (1) outside 0.3 Mpc the mass-to-light ratio is almost constant for all the clusters in the sample, and (2) the distribution of M/L_V values, at $r = 1.5$ Mpc h_{50}^{-1}, is peaked around the value 137 $M_\odot/L_\odot$, with an rms spread of 52 $M_\odot/L_\odot$. This spread includes the effect of the temperature uncertainty. This value of M/L_V is comparable to the findings of Cowie et al. (1987) and David et al. (1995). Thus we add a piece of statistical evidence in favor of an average M/L_V value smaller than the value deduced from optical data which lies in the range 200–300 h_{50} (e.g., Faber & Gallagher 1979).

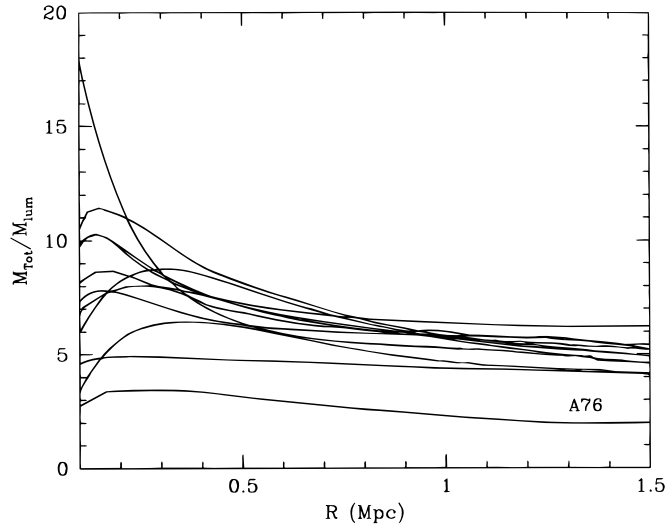

FIG. 6.—Ratio between total and luminous matter for the cluster sample, as a function of radius.

We can also compute the dark mass by subtracting from the total binding mass the masses of gas and galaxies: $M_{\rm dark} = M_{\rm tot} - M_{\rm gas} - M_{\rm gal}$. The ratio of dark mass to the galactic mass behaves qualitatively like M/L_V. Thus, for radii $\gtrsim 250\ h_{50}^{-1}$ kpc the galactic matter closely traces the cluster dark matter.

Measuring the ratio $M_{\rm dark}/M_{\rm gal}$ at respectively 0.15 and 1.5 Mpc and taking the ratio η of these two values, we find that on average $\eta = 0.98$ in the case of a fit with the de Vaucouleurs profile. In the case of the King profile we find $\eta = 2.3$, which would correspond to an excess of dark matter in the cluster center. However, the de Vaucouleurs profile provides a better representation of the galaxy distribution, as discussed in § 2.2. Thus the central excess of dark matter could be simply an artifact due to the use of the King profile approximation. To check this further, we have also compared the projected total and gas masses with the galaxy mass deduced from two-dimensional galaxy counts, avoiding any parameterization of the galaxy distribution. The resulting mass profiles provide strong evidence in favor of the de Vaucouleurs profile with respect to the King profile. Thus we conclude that there is no evidence for a real excess of dark matter with respect to galactic mass in the central region of clusters.

Another interesting quantity is the ratio between the total binding mass and the luminous mass $M_{\rm lum}$, consisting of gas plus galaxies, which is shown in Figure 6. Also in this case the differences among individual clusters decrease at large radii. At $r = 1.5$ Mpc, $M_{\rm tot}/M_{\rm lum}$ is 5.0 ± 0.8 excluding A76, which is an irregular cluster with the lowest temperature in the list of David et al. (1993) and with a large uncertainty.

Since an unknown fraction of the dark matter is baryonic, the luminous fraction $M_{\rm lum}/M_{\rm tot}$ represents a lower limit to the baryonic fraction f_b of the total mass. Previous studies have shown that the luminous fraction tends to increase to about 0.3 in the outer ($r > 2$ Mpc) regions (Briel et al. 1992; Elbaz, Arnaud, & Böhringer 1995; David et al. 1995). Thus our average value $M_{\rm lum}/M_{\rm tot} = 0.20$ represents an estimate of the lower limit to the baryonic fraction inside galaxy clusters. This limit is further lowered by adopting a lower value of the galaxy mass-to-light ratio as suggested by more recent estimates (van der Marel 1991). Using conservatively $M/L_V = 3\ M_\odot/L_\odot$, we obtain $M_{\rm lum}/M_{\rm tot} = 0.19$, only slightly different from the previous estimate because the gas mass dominates the luminous mass at large radii. Considering this value as universal (see White 1992; White et al. 1993), we can derive the corresponding limit on the cosmological parameter Ω_0 using the limit on the universal baryonic fraction $\Omega_b^{\rm nucl} = 0.05\ h_{50}^{-2}$ resulting from primordial nucleosynthesis calculations (Walker et al. 1991). From our lower limit on f_b we obtain $\Omega_0 = \Omega_b/f_b \leq 0.25$, a value consistent with David et al. (1995).

4. CONCLUSIONS

We have carried out a combined X-ray and optical study for a sample of 12 galaxy clusters.

From the optical data we have derived the total luminosity of each cluster and the galaxy number density distributions. These have been fitted with both King and de Vaucouleurs profiles. The latter representation provides, on

average, a better fit, indicating a possible excess of radial orbits in the cluster center.

The X-ray surface brightness has been deprojected using both parametric and nonparametric techniques. The results are very similar, indicating that the parameterization does not introduce significant biases, at least within 1.5 Mpc.

Since the signal-to-noise ratio is intrinsically limited in the case of galaxy counts, the noise amplification in the nonparametric deprojection becomes prohibitive. Thus we have compared parametric deprojections based on maximum likelihood fit with either de Vaucouleurs or King density profiles. The two parameterizations are almost equivalent at large radii, but the former gives a better representation in the central region.

The comparison between the gas density $\rho_{\rm gas}$ and the galaxy density $\rho_{\rm gal}$ shows that $\rho_{\rm gas} \propto \rho_{\rm gal}^{\beta}$ consistently with the prediction of the hydrostatic isothermal model.

A study of the mass distribution as a function of radius shows that, despite the differences among individual clusters, there is a uniform qualitative behavior of the various matter components: (1) more than 70% of the total mass is dark (within 1.5 Mpc), and (2) the gas is diffused in a larger volume with respect to galaxies and dark matter.

The mass-to-light ratio is almost constant outside $\approx$250 kpc, and the average value for the sample is 137 ± 52 $M_{\odot}/L_{\odot}$.

The ratio $M_{\rm lum}/M_{\rm tot}$ of the luminous over the total mass of different clusters tends roughly to the same value, which provides a lower limit to the baryon fraction inside clusters $f_b \gtrsim 0.2$.

Under the assumption that the cosmic density parameter Ω_0 is not much smaller than the unit, and using the limits on Ω_b provided by nucleosynthesis calculations, the above limit on f_b would imply $\Omega_b \approx f_b > \Omega_b^{\rm nucl}$, namely, that baryons must be preferentially concentrated inside galaxy clusters.

Alternatively, if we assume that the baryon fraction at $r \gtrsim 1.5$ Mpc is representative of the cosmic value, our results constrain Ω_0 to be smaller than 0.25.

The gas mass is not strongly dependent on the temperature. Our estimate of the total binding mass within $R = 1.5$ Mpc could be substantially modified only by large changes of the temperature in the outer regions. Recent results based on *ASCA* observations of the cluster A2163 (Markevitch et al. 1996) do in fact indicate a significant temperature decrease for $R > 2$ Mpc, but at the same time they show that a constant temperature is consistent with the data within $R = 1.5$ Mpc. Only further, spatially resolved, spectroscopic observations of the outer and fainter regions of galaxy clusters will provide new detailed information on their structure, on the cosmic value of the baryon fraction, and consequently on the cosmological density parameter Ω_0.

We are grateful to A. Cavaliere and to G. C. Perola for useful discussions and comments. We acknowledge grants from CNR and MURST. G. C. was partly supported by a CNR fellowship.

REFERENCES

Abramopoulos, F., & Ku, W. H. M. 1983, ApJ, 271, 446
Allen, S. W., Fabian, A. C., Edge, A. C., Böhringer, H., & White, D. A. 1995, MNRAS, 275, 741
Bahcall, N. A., & Lubin, L. M. 1994, ApJ, 426, 513
Briel, U. G., Henry, J. P., & Böhringer, H. 1992, A&A, 259, L31
Cavaliere, A., & Fusco-Femiano, R. 1976, A&A, 49, 137
Cowie, I. L., Henriksen, M., & Mushotzky, R. 1987, ApJ, 317,593
David, L. P., Arnaud, K. A., Forman, W., & Jones, C. 1990, ApJ, 356, 32
David, L. P., Jones, C., & Forman, W. 1995, ApJ, 445, 578
David, L. P., Slyz, A., Jones, C., Forman, W., Vrtilek, D., & Arnaud, K. A. 1993, ApJ, 412, 479
Durret, F., Gerbal, D., Lachièze-Rey, M., Lima-Neto, G., & Sadat, R. 1994, A&A, 287, 733
Elbaz, D., Arnaud, M., & Böhringer, H. 1995, A&A, 293, 337
Evrard, A. E., Metzler, C. A., & Navarro, J. F. 1995, preprint, astro-ph/9510058
Eyles, C. J., Watt, M. P., Bertram, D., & Church, M. J. 1991
Faber, S. M., & Gallagher, J. S. 1979, ARA&A, 17, 135
Flin, P., Trèvese, D., Cirimele, G., & Hickson, P. 1995, A&AS, 110, 313
Gerbal, D., Durret, F., Lima-Neto, G., & Lachièze-Rey, M. 1992, A&A, 253, 77
Girardi, M., Fadda, D., Giuricin, G., Mardirossian, F., Mezzetti, M., & Biviano, A. 1996, ApJ, 457, 61
Hasinger, G., et al. 1993, A&A, 275, 1
Hughes, J. P. 1989, ApJ, 337, 21
Hughes, J. P., Gorenstein, P., & Fabricant, D. 1988, ApJ, 329, 82
Jones, C., & Forman, W. 1984, ApJ, 276, 38
Markevitch, M., Mushotzky, R., Inoue, H., Yamashita, K., Furuzawa, A., & Tawara, Y. 1996, ApJ, 456, 437
Oemler, A., Jr. 1974, ApJ, 194, 1
Plucinsky, P. P., Snowden, S. L., Briel, U. G., Hasinger, G., & Pfeffermann, E. 1993, ApJ, 418, 519
Raymond, J. C., & Smith, B. W. 1977, ApJS, 35, 419
Rood, H. J., & Sastry, G. 1971, PASP, 83, 313
Sarazin, C. L. 1988, X-Ray Emissions from Clusters of Galaxies (Cambridge: Cambridge Univ. Press)
Schindler, S. 1996, A&A, 305, 756
Schneider, D., P., Gunn, J. E., & Hoessel, J. G. 1983, ApJ, 264, 337
Smail, I., Ellis, R. S., Fitchett, M. J., & Edge, A. C. 1995, MNRAS, 273, 277
Snowden, S. L., Plucinsky, P. P., Briel, U., Hasinger, G., & Pfeffermann, E. 1992, ApJ, 393, 819
Stark, A. A., Gammie, C. F., Wilson, R. W., Bally, J., Linke, R. A., Heiles, C., & Hurwitz, M. 1992, ApJS, 79, 77
Struble, M. F., & Rood H. J. 1991, ApJS, 77, 363
Tonry J. L. 1985, ApJ, 291, 45
Trèvese, D., Cirimele, G., & Appodia, B. 1996, A&A, in press
Trèvese, D., Cirimele, G., & Flin, P. 1992a, AJ, 104, 3
Trèvese, D., Flin, P., Migliori, L., Hickson, P., & Pittella, G. 1992b, A&AS, 94, 327 (T92)
Tyson, A. J., Valdes, F., & Wenk, R. A. 1990, ApJ, 349, L1
van der Marel, R. P. 1991, MNRAS, 253, 710
Walker, T. P., Steigman, G., Schramm, D. N., Olive, K. A., & Kang, H. 1991, ApJ, 376, 51
White, S. D. M. 1992, in Clusters and Superclusters of Galaxies, ed. A. C. Fabian (Dordrecht: Kluwer), 17
White, S. D. M., Navarro, J. F., Evrard, A. E., & Frenk, C. S. 1993, Nature, 366, 429